RMetS

Royal Meteorological Society

Synoptic and mesoscale processes supporting vertical superposition of the polar and subtropical jets in two contrasting cases

Andrew C. Winters[a] and Jonathan E. Martin[b*]

[a]Department of Atmospheric and Environmental Sciences, University at Albany – State University of New York, USA
[b]Department of Atmospheric and Oceanic Sciences, University of Wisconsin-Madison, USA

*Correspondence to: J. E. Martin, Department of Atmospheric and Oceanic Sciences, University of Wisconsin-Madison, 1225 W. Dayton Street, Madison, WI 53706, USA. E-mail: jemarti1@wisc.edu

Observational studies have shown that the tropopause characteristically exhibits a three-step Pole-to-Equator structure, with each break between steps in the tropopause height associated with a jet stream. While the two jet streams, the polar and subtropical jets, typically occupy different latitude bands, their separation can occasionally vanish, resulting in a relatively rare vertical superposition of the two jets. A cursory examination of several historical and recent high-impact weather events over North America and the North Atlantic suggests that superposed jets are a component of their evolution. This study examines the processes that support the production of a polar/subtropical jet superposition during two such events; the 18–20 December 2009 Mid-Atlantic Blizzard and the 1–3 May 2010 Nashville Flood.

Given that ageostrophic transverse circulations and convection have both been shown to be capable of restructuring the tropopause within a single jet environment, the analysis focuses on the role these same processes play within the more complex double-jet environment. The results demonstrate that ageostrophic transverse circulations play a primary role in the production of a superposition during the December 2009 case by placing subsidence, and a downward protrusion of high potential vorticity (PV) air, between the two jet cores, thereby contributing to the production of the single, steep tropopause wall characteristic of the superposed jet environment. Furthermore, convection fundamentally influences the existence and structure of the subtropical jet stream in both cases, through its associated latent heat release and irrotational outflow as well as the geostrophic adjustment process that responds to upper-tropospheric mass deposition from convection on the anticyclonic shear side of the jet.

Key Words: jet streams; ageostrophic transverse circulations; convection

Received 24 April 2015; Revised 18 November 2015; Accepted 20 November 2015; Published online in Wiley Online Library 9 February 2016

1. Introduction

Narrow, rapidly flowing currents of air located near the tropopause are known as jet streams or jets. These jets, often found nearly girdling the globe while exhibiting large meridional meanders, are among the most recognizable structural characteristics within the Earth's atmosphere. Careful observational work by Defant and Taba (1957, hereafter DT57) was one of the first to demonstrate that the location of these jets is intricately related to the structure of the tropopause. Specifically, they found that the atmosphere typically exhibits the three-step Pole-to-Equator tropopause structure[†] shown in Figure 1, wherein each step is separated from its neighbours by

the presence of a westerly wind maximum (Winters and Martin, 2014, their Fig. 2). In particular, the subtropical jet resides within the break between the tropical ($\sim$90 hPa) and subtropical ($\sim$250 hPa) tropopauses at the poleward edge of the Hadley cell and is characterized by relatively modest baroclinicity in the upper troposphere and lower stratosphere (e.g. Loewe and Radok, 1950; Yeh, 1950; Koteswaram, 1953; Mohri, 1953; Koteswaram and Parthasarathy, 1954; Sutcliffe and Bannon, 1954; Krishnamurti, 1961; Riehl, 1962). The polar jet is located farther poleward ($\sim$50°N in the Northern Hemisphere) in the break between the subtropical tropopause and the even lower polar tropopause ($\sim$300 hPa) and is positioned atop the strongly baroclinic, tropospheric-deep polar front (e.g. Palmén and Newton, 1948,

---

[†]DT57 identified the tropopause via the analysis of soundings. The tropopause was identified at the elevation of a 'noticeable change of tropospheric lapse rate

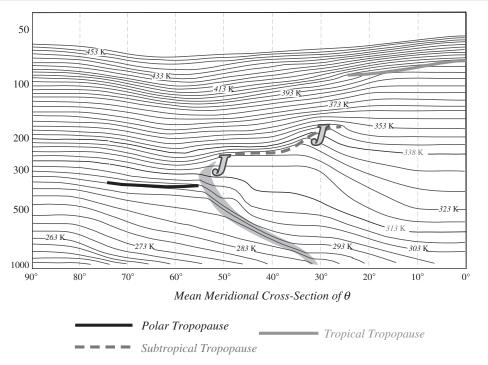to an isothermal layer or to an increase of temperature with height' (DT57, p. 261).

Figure 1. Mean meridional cross-section (latitude/pressure in hPa) of potential temperature for 1 January 1956 with the polar, subtropical and tropical tropopauses labelled as indicated in the legend. The polar frontal layer is shaded in grey. From Winters and Martin (2014), their Fig. 2.

1969; Namias and Clapp, 1949; Newton, 1954; Keyser and Shapiro, 1986; Shapiro and Keyser, 1990).

A particularly insightful element of the DT57 analysis was their construction of hemispheric maps of tropopause height (in hPa). One such map, shown in Figure 2 (Winters and Martin, 2014, their Fig. 3), demonstrates that the location of the individual tropopause breaks, and thus the jets at any particular time, are characterized by sharp, localized, and easily identifiable gradients in tropopause height. While the analysis indicates that the polar and subtropical jets typically occupy different latitude bands, substantial meanders in their location are common. Occasionally, the characteristic meridional separation between the two jets can vanish, as it does in Figure 2 in the area bounded by the black circle over the North Atlantic, where the polar and subtropical jets vertically superpose.[‡] The consequences of such a vertical superposition are the development of a two-step tropopause structure from the Tropics to high latitudes, rather than the more common three-step structure represented in Figure 1, and a consolidation of the upper-tropospheric and lower-stratospheric baroclinicity associated with each jet into a substantially narrower zone of contrast. Together, these observations of the tropopause by DT57 are specifically identified as the theoretical foundation to an objective jet identification scheme outlined in Winters and Martin (2014, hereafter WM14).

Employing that jet identification scheme as part of an analysis of the 1–3 May 2010 Nashville (TN) Flood, WM14 found that the event was characterized by the development of a superposed jet. As the jets became superposed, WM14 diagnosed a strengthening of the associated ageostrophic transverse circulation. The low-level, poleward-directed branch of this circulation was subsequently found to make the primary contribution to an observed increase in poleward moisture flux over the southeastern United States that preceded the second day of heavy rainfall characterizing the 2010 Nashville Flood. Moore *et al.* (2012) indicated that this increase in poleward moisture flux was essential for the continued production of heavy precipitation during the latter half of the

event. In light of this result, the analysis by WM14 highlighted one specific pathway through which a superposed jet, and its associated ageostrophic transverse circulation, can influence the evolution of a high-impact weather event.

In addition to the 2010 Nashville Flood, a cursory examination of a number of other historical and recent high-impact weather events over North America and the North Atlantic by the authors suggests that superposed jets were a component of their evolution. For example, Defant (1959) discussed the impact of a dramatic jet superposition on an explosive cyclogenesis event south of Iceland on 8 January 1956, in which the sea-level pressure dropped 61 hPa in 24 h. Furthermore, the 25–26 January 1978 Cleveland Superbomb (Hakim *et al.*, 1995, their Fig. 5), the 15–16 October 1987 Great October Storm (Hoskins and Berrisford, 1988, their Fig. 7), the 12–14 March 1993 Storm of the Century (Bosart *et al.*, 1996, their Fig. 13), the 18–20 December 2009 Mid-Atlantic (States) Blizzard (National Weather Service, 2014), and the 25–28 April 2011 severe weather outbreak (Christenson and Martin, 2012) are all examples of events that occurred within an environment that exhibited the two-step tropopause structure associated with a superposed jet.

The association of jet superpositions with a class of high-impact weather events, and the relatively infrequent occurrence of superpositions over North America and the North Atlantic (Christenson, 2013), motivates an investigation into the mechanisms that support the process of superposition. This topic was not considered as part of the previous work by WM14 and remains an outstanding research question. Historically, prior work that addresses the related topic of jet 'mergers' has been focused on either interannual or climatological time-scales (e.g. Lee and Kim, 2003; Son and Lee, 2005; Eichelberger and Hartmann, 2007; Harnik *et al.*, 2014), has been strongly based on wave–wave interaction (e.g. Lee and Kim, 2003; Son and Lee, 2005; Martius *et al.*, 2010; O'Rourke and Vallis, 2013), and/or has been conducted within an idealized model environment (e.g. Lee and Kim, 2003; Son and Lee, 2005; O'Rourke and Vallis, 2013). This circumstance, coupled with only limited analysis of such features using actual observed data, has resulted in incomplete insight into the synoptic–dynamic mechanisms that foster the development of jet superpositions.

The concept of midlatitude trough mergers (e.g. Lai and Bosart, 1988; Gaza and Bosart, 1990; Hakim *et al.*, 1995; Dean and Bosart, 1996; Hakim *et al.*, 1996; Strahl and Smith, 2001), in which two

---

[‡]More recently, potential vorticity (PV) tropopause maps have also been beneficial in locating the individual tropopause breaks and the occasional vertical superposition of the polar and subtropical jets (e.g. Hoskins and Berrisford, 1988; Davis and Emanuel, 1991; Hakim *et al.*, 1995; Bosart *et al.*, 1996; Morgan and Nielsen-Gammon, 1998; Shapiro *et al.*, 1999).
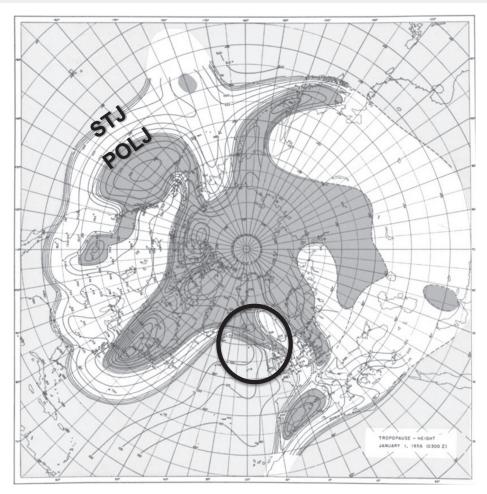
Figure 2. Northern Hemispheric map of tropopause height (hPa) at 0300 UTC 1 January 1956. Tropopause breaks that correspond to the subtropical jet (STJ) and polar jet (POLJ) are labelled accordingly. The area identified with a circle is a region characterized by a vertical superposition of the polar and subtropical jets. Dark grey shading corresponds to the polar tropopause, white shading to the subtropical tropopause, and light grey to the tropical tropopause. From Winters and Martin (2014), their Fig. 3.
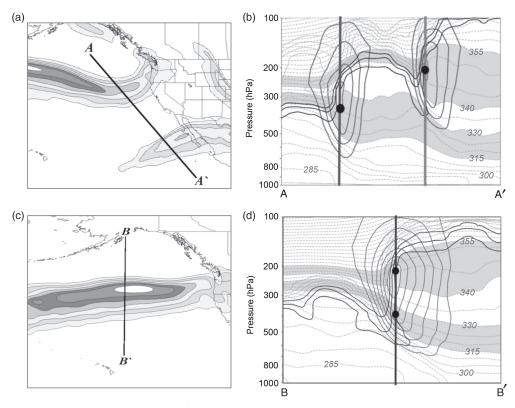

Figure 3. (a) The 300 hPa wind speeds (shaded every 10 m s^{-1} starting at 30 m s^{-1}) at 0000 UTC 27 April 2010 depicting separate polar and subtropical jets. (b) Cross-section A-A', in Figure 3(a), through separate polar and subtropical jet cores with contours of 1-, 2- and 3-PVU (black); 4-, 5-, 6-, 7-, 8- and 9-PVU (light grey); potential temperature every 5 K (dashed grey); and wind speed every 10 m s^{-1} beginning at 30 m s^{-1} (dark grey). The 315–330 and 340–355 K isentropic layers, used to identify the locations of the jets, are shaded grey. The dark vertical lines correspond to grid columns with the black dot confirming a positive identification of a polar or subtropical jet. (c) As in (a), but for a superposed jet at 0000 UTC 24 October 2010. (d) As in (b), but for the cross-section B-B', in Figure 3(c), with two positive identifications (black dots) within a single grid column indicating a jet superposition. From Winters and Martin (2014), their Fig. 4.

mid-tropospheric vorticity maxima with origins in distinctly different westerly airstreams amalgamate into a single maximum, offers the closest physical analogue to jet superpositions in the synoptic–dynamic literature. While it appears that certain trough merger cases may be simultaneously characterized by jet superpositions, the aforementioned studies do not identify the merging air streams as distinctly related to separate polar and subtropical jets and do not specifically investigate the impact of trough merger on the evolution of the upper-tropospheric jet and tropopause structure. Instead, the focus of these studies is largely placed on the effects a merger can have on the development of surface cyclones.

Numerous observationally based studies have addressed the different mechanisms that can be responsible for altering the structure of an *individual* jet stream, however. For instance, the presence of ageostrophic transverse circulations, and particularly the differential vertical motions associated with them in the vicinity of an upper-level jet-front system, can act not only to aid in the production of precipitation, but also to significantly restructure the baroclinicity and tropopause both above and below the jet. Many of the historical contributions to the problem of upper-tropospheric frontogenesis are well summarized by Keyser and Shapiro (1986), while Lang and Martin (2012) provide a recent extension of these studies to the process of lower-stratospheric frontogenesis.

The influence of convection in altering the structure of the tropopause on the anticyclonic shear side of a jet has also been well documented. In particular, Lang and Martin (2013) investigated four cases of upper-frontal evolution in southwesterly flow. They noted that latent heat release offers separate but simultaneous physical mechanisms that can alter the tropopause structure. First, direct diabatic erosion of potential vorticity (PV) above the heating maximum can increase the tropopause height in a given column. Second, the associated reduction in upper-tropospheric static stability can intensify a forced ageostrophic transverse circulation, which can then act to further tilt the tropopause. Tropical cyclones and extratropical transition (ET) events have also been shown to exert a considerable influence on the location and strength of the subtropical jet via the negative PV advection accomplished by their tropopause-level, divergent outflow and the diabatic erosion of upper-tropospheric PV that accompanies intense latent heat release in the middle troposphere (e.g. McTaggart-Cowan *et al.*, 2001, 2004, 2007; Agusti-Panareda *et al.*, 2004; Ahmadi-Givi *et al.*, 2004; Grams *et al.*, 2011, 2013; Archambault *et al.*, 2013, 2015; Griffin and Bosart, 2014).

Despite extensive research on a variety of aspects of upper-level jet-front systems, no prior study has examined the role of the above dynamical mechanisms in specifically supporting the interaction and subsequent vertical superposition of the two, initially distinct, jet features. Consequently, the present study will consider the specific roles that ageostrophic transverse circulations, convection, and the interaction between the two may play in the restructuring of the tropopause that characterizes jet superpositions. These objectives stand in contrast to WM14, which focused solely on the specific role that a superposed jet's ageostrophic transverse circulation played in magnifying a high-impact event. The process of superposition will be addressed through the examination of two recent high-impact weather events associated with superposed jets: the 18–20 December 2009 Mid-Atlantic Blizzard and the aforementioned 1–3 May 2010 Nashville Flood. These events were selected because they occurred at different times of the year and were associated with different types of high-impact weather event (i.e. rapid cyclogenesis and an extreme precipitation event).

The remainder of this study is structured as follows. Section 2 briefly discusses the WM14 jet identification scheme, given its relevance to the current study, and provides some background on the Sawyer–Eliassen circulation equation (Sawyer, 1956; Eliassen, 1962), which is used to diagnose the ageostrophic transverse jet circulations. Sections 3 and 4 diagnose the development

Upper Troposphere

Figure 4. Idealized configurations of jet circulations associated with a straight jet streak on an isobaric surface in the upper troposphere. Geopotential height (thick solid lines), potential temperature (dashed lines), geostrophic wind speed (fill pattern, with the jet speed maximum represented by the J), and Sawyer–Eliassen vertical motions indicated by 'Up' and 'Down' for a regime of (a) no geostrophic temperature advection, (b) upper-tropospheric geostrophic cold-air advection, and (c) upper-tropospheric geostrophic warm-air advection along the jet axis. From Lang and Martin (2012), their Fig. 3.

of a superposed jet during each individual case, respectively, and section 5 finishes with a discussion and suggestions for future work.

2. Methodology

This study is performed using model analyses from the National Centers for Environmental Prediction (NCEP) Global Forecast System (GFS) at 6 h intervals with a horizontal grid spacing of $1.0° \times 1.0°$ and a vertical grid spacing of 50 hPa (25 hPa between 1000 and 900 hPa). To accommodate the jet identification scheme outlined in WM14, which is briefly summarized below, these data were bilinearly interpolated onto isentropic surfaces at 5 K intervals from 300 to 370 K using programs within the General Meteorological Package (GEMPAK: desJardins *et al.*, 1991). Throughout the subsequent analysis, the tropopause will refer to the location of the 2-PVU surface (1 PVU $= 10^{-6}$ K m^2 kg^{-1} s^{-1}), in line with defining the dynamic tropopause as a surface of constant PV (e.g. Morgan and Nielsen-Gammon, 1998). With this definition for the dynamic tropopause, and in an effort to better diagnose its movement, PV advection is calculated using only the gradient in the 1−3-PVU channel.

2.1. Jet identification

The forthcoming summary of the identification scheme for the polar, subtropical, and superposed jet streams[§] contains elements from WM14 and references the features shown in Figure 3 (WM14, their Fig. 4). Figure 3(a) depicts a characteristic example of clearly separate polar and subtropical jets from 0000 UTC 27

[§]Throughout the course of this study, the term jet 'stream' is synonymous with jet 'streak' and will refer to a zonally confined wind speed maximum along either the polar or subtropical waveguide.

April 2010 in the eastern North Pacific. A vertical cross-section A-A′ through these distinct features unambiguously identifies the separate jet cores and a three-step tropopause structure (Figure 3(b)). From this cross-section, it is apparent that the polar jet core, located at approximately 300 hPa, is largely contained within the 315−330 K isentropic layer, while the subtropical jet core occupies the 340−355 K isentropic layer at roughly 200 hPa. Additionally, both the polar and the subtropical jets lie at the low PV edge of the strong horizontal PV gradient that separates the upper troposphere from the lower stratosphere in their respective isentropic layers. With these attributes in mind, the identification scheme identifies the presence, or absence, of a polar or subtropical jet within each grid column based upon whether the wind speed distribution and horizontal PV gradient within each jet's isentropic layer satisfy the criteria specified in WM14.¶ The occurrence of both polar and subtropical jet characteristics in a single grid column identifies a jet superposition at that time in that grid column. An example of a jet superposition is shown in Figure 3(c) at 0000 UTC 24 October 2010. Notice that, rather than the three-step tropopause structure shown in Figure 3(b), a superposed jet is characterized by a two-step tropopause structure with a steep tropopause wall that extends from the polar to the tropical tropopause (Figure 3(d)). This nearly vertical PV wall (from roughly 550 to 150 hPa in this example case) is the leading structural characteristic of a superposed jet.

2.2. Sawyer−Eliassen circulation equation

A particularly powerful diagnostic tool for interrogating the ageostrophic transverse circulations associated with jet-front structures, in nearly straight flow, is afforded by the Sawyer−Eliassen circulation equation (Sawyer, 1956; Eliassen, 1962)‖:

$$\left(-\gamma\frac{\partial\theta}{\partial p}\right)\frac{\partial^2\psi}{\partial y^2} + \left(2\frac{\partial M}{\partial p}\right)\frac{\partial^2\psi}{\partial p\partial y} + \left(-\frac{\partial M}{\partial y}\right)\frac{\partial^2\psi}{\partial p^2}$$
$$= Q_g - \gamma\frac{\partial}{\partial y}\left(\frac{d\theta}{dt}\right), \tag{1}$$

where γ is a constant on isobaric surfaces [$\gamma = (R/fp_o)(p_o/p)^{c_v/c_p}$], $p_o = 1000$ hPa, $c_v = 718$ J kg^{-1} K^{-1}, $c_p = 1004$ J kg^{-1} K^{-1}, R is the gas constant for dry air, θ is the potential temperature, and f is the Coriolis parameter. In addition, Q_g is the geostrophic forcing term, which is the sum of the shearing [$Q_{SH} = 2\gamma\{(\partial U_g/\partial y)(\partial\theta/\partial x)\}$] and stretching deformation terms [$Q_{ST} = 2\gamma\{(\partial V_g/\partial y)(\partial\theta/\partial y)\}$] and where U_g and V_g are the along- and across-front geostrophic winds. M is defined as the absolute geostrophic momentum ($M = U_g - fy$). The coefficients of the second-order terms on the left-hand side of Eq. (1) represent the static stability, baroclinicity, and inertial stability, respectively, and act to modulate the structure of the ageostrophic transverse circulation. The ageostrophic transverse circulation lies in a plane perpendicular to the frontal boundary (i.e. jet axis) and is determined by the Sawyer−Eliassen stream function, ψ, such that the across-front ageostrophic wind and vertical motion are defined as $v_{ag} = -\partial\psi/\partial p$ and $\omega = dp/dt = \partial\psi/\partial y$, respectively. In the solution, the along-front component of the ageostrophic circulation (u_{ag}) is assumed to be zero. For the purposes of this study, successive over-relaxation (SOR) is used to converge on a solution to Eq. (1) for the ageostrophic transverse circulation following the method described in WM14. The reader is referred

to Eliassen (1962) or Keyser and Shapiro (1986) for the full derivation and a more detailed discussion of Eq. (1).

Employing Eq. (1), Shapiro (1982) described a series of conceptual models detailing the characteristic transverse circulations associated with idealized upper-level jet-front systems. Specifically, in the absence of any along-jet geostrophic temperature advection, solutions for the ageostrophic circulations are driven purely by the geostrophic stretching deformation and resembled the traditional four-quadrant model, with a thermally direct (indirect) circulation in the jet-entrance (-exit) region (Figure 4(a)). The introduction of along-jet geostrophic temperature advection mobilizes the geostrophic shearing deformation term, which acts to 'shift' the thermally direct (indirect) circulation to the anticyclonic (cyclonic) shear side of the jet in cases of geostrophic cold-air advection, such that subsidence is present through the jet core (Figure 4(b)). Conversely, geostrophic warm-air advection along the jet axis shifts the thermally direct (indirect) circulation to the cyclonic (anticyclonic) shear side of the jet, positioning ascent through the jet core (Figure 4(c)).**

3. Jet evolution during the 18−20 December 2009 Mid-Atlantic Blizzard

3.1. Synoptic overview

Throughout the 72 h period of 18−20 December 2009, large portions of the Mid-Atlantic and New England states accumulated 30−60 cm of snow in conjunction with a rapidly deepening midlatitude cyclone that formed over the northern Gulf of Mexico and tracked northeastward along the East Coast of the USA (National Weather Service, 2014). Coincident with the cyclone's most rapid period of intensification was the development of a jet superposition over the southeastern United States. For brevity, the following overview will focus primarily on the jet evolution in the upper troposphere in the hours preceding superposition.

At 0000 UTC 19 December, 36 h prior to jet superposition, a subtropical jet (red dashed line) with winds in excess of 60 m s^{-1} extended from central Mexico northeastward across the Florida peninsula, while a weaker polar jet (blue dashed line) was identified upstream of a polar trough in northwesterly flow over the Central Plains (Figure 5(a)). A cross-section through the two separate jet structures at this time (Figure 5(b)) indicates the presence of a three-step tropopause structure and demonstrates that the jets were clearly distinct from one another. The developing midlatitude cyclone responsible for producing blizzard conditions across much of the eastern United States was also firmly located in a favourable position for further deepening in the subtropical jet's left exit region.

By 1800 UTC 19 December, the subtropical jet was displaced slightly poleward of its previous location and was noticeably stronger, with winds now in excess of 80 m s^{-1} (Figure 5(c)). The surface cyclone, which had deepened by roughly 8 hPa, remained favourably located within the subtropical jet's left exit region off the Mid-Atlantic coast, suggesting that the jet likely played a role in the cyclone's development. Meanwhile, the polar jet, which was also characterized by increased wind speeds, had propagated around the base of the deepening polar trough and had assumed an orientation parallel to the subtropical jet over the southeastern United States. A cross-section through the entrance regions of both of these jet structures (Figure 5(d)) indicates the persistence of a three-step tropopause structure and that the two jets, while in closer proximity to one another by this time, were still not vertically superposed.

During the subsequent 18 h, the cyclone underwent its most rapid period of intensification, reaching a minimum central

---

¶A polar (subtropical) jet is identified at a grid point if the magnitude of the horizontal PV gradient within the 1−3-PVU channel exceeds 1.4×10^{-5} PVU m^{-1} (0.9×10^{-5} PVU m^{-1}) in the 315−330 K (340−355 K) isentropic layer and the 400 to 100 hPa integrated wind speed is greater than 30 m s^{-1}.

‖Equation (1) is shown in isobaric coordinates, which offers the advantage of distinguishing between the geostrophic and diabatic forcing terms.

**These circulations are fortified by ascent and descent associated with positive and negative vorticity advection by the thermal wind (i.e. Sutcliffe, 1947) as described by Martin (2014).
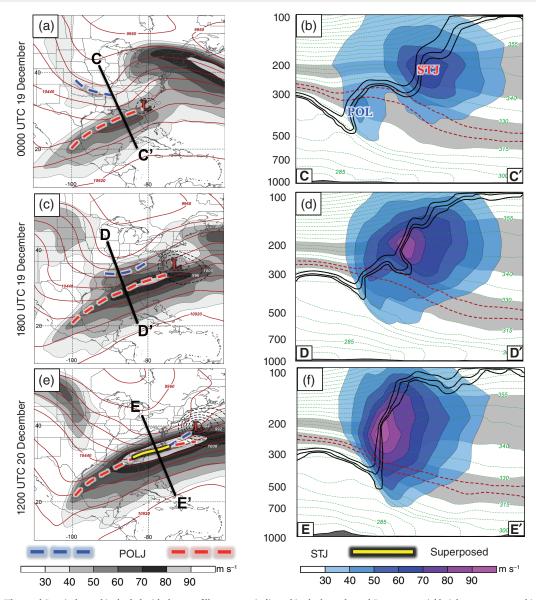
Figure 5. (a,c,e) The 250 hPa wind speed is shaded with the grey fill pattern as indicated in the legend, 250 hPa geopotential heights are contoured in red every 120 m, sea-level pressure is contoured with the dashed black lines every 4 hPa below 1000 hPa, the location of the sea-level pressure minimum is identified with the red 'L', and jet axes (identified with reference to the WM14 jet identification scheme) are identified as specified in the legend, for (a) 0000 UTC 19 December, (c) 1800 UTC 19 December, and (e) 1200 UTC 20 December 2009. (b,d,f) Cross-sections, as identified in the plot immediately to its left, of wind speed shaded in the blue fill pattern according to the legend, potential temperature contoured every 5 K (dashed green lines), and contours of 1-, 2- and 3-PVU (black) at (b) 0000 UTC 19 December, (d) 1800 UTC 19 December, and (f) 1200 UTC 20 December 2009. The grey shaded isentropic layers are those used to identify the jet axes using the identification scheme outlined in the text and the 320 and 325 K isentropes are highlighted with the dashed red lines in the cross-sections for reasons discussed in the text.

pressure below 980 hPa southeast of Cape Cod at 1200 UTC 20 December (Figure 5(e)). Coincident with this period of most rapid intensification was a superposition of the polar and subtropical jets from central Georgia northeastward to off the North Carolina coast (yellow line). This superposed jet was characterized by increased wind speeds, now well in excess of 90 m s^{-1}, and was positioned such that the cyclone remained firmly located in the jet's left exit region. An investigation of the movement of each individual jet axis from the previous time indicates that the subtropical jet was, once again, displaced only slightly poleward of its prior location, while the polar jet was located farther southeast of its previous position, consistent with the continued propagation and deepening of the polar trough.

A cross-section drawn through the superposed portion of this jet illustrates the two-step tropopause structure and vertical PV wall (extending from roughly 500 to 150 hPa) characteristic of a superposed jet (Figure 5(f)). Consistent with this structure, the cross-section no longer depicts two separate wind speed maxima, but rather a single jet core with wind speeds in excess of 90 m s^{-1}. Particular attention is drawn to the 320 and 325 K isentropes, highlighted in red, which are located at a significantly lower altitude beneath the jet core than at the prior times (Figure 5(b,d)).

This suggests that subsidence may have been responsible for the downward depression of these isentropes during the intervening 18 h and, therefore, potentially played a role in restructuring the tropopause into the characteristic superposed jet structure. The veracity of this inference is considered as part of the subsequent analysis.

3.2. Superposed jet formation

3.2.1. Subtropical jet evolution

Given that polar and subtropical jets are each associated with unique tropopause breaks, insight into the formation of a superposed jet can be garnered through a diagnosis of the movement of each individual tropopause break (i.e. jet axis), as they eventually become vertically aligned. In this case, the existence of a subtropical jet was closely tied to the presence of remote tropical convection over portions of Central America and the eastern equatorial Pacific Ocean. One particularly insightful way to examine the effect that tropical convection can have on the subsequent evolution of the subtropical jet is through a consideration of the anomalous pressure depth of the isentropic
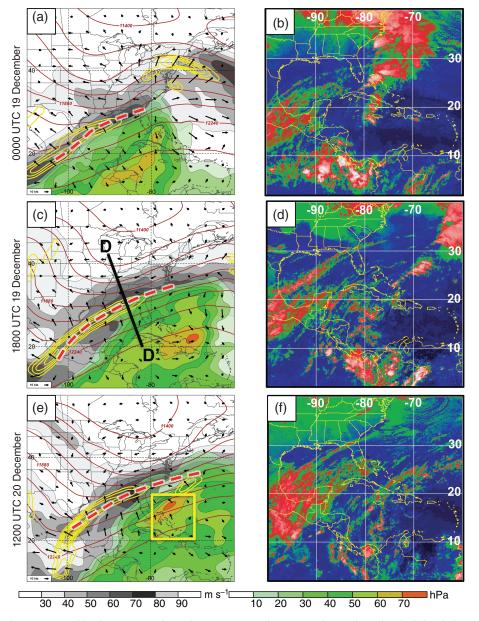
Figure 6. (a,c,e) The 200 hPa geopotential height is contoured in red every 120 m, 200 hPa geostrophic wind speed is shaded with the grey fill pattern according to the legend, positive perturbation pressure depths within the 340–355 K isentropic layer are shaded in the green fill pattern according to the legend, negative PV advection within the 1−3-PVU channel by the divergent wind (arrows) is contoured in yellow every 2×10^{-5} PVU s^{-1}, and the subtropical jet axis from Figure 5 is identified with the thick, dashed red line for (a) 0000 UTC 19 December, (c) 1800 UTC 19 December, and (e) 1200 UTC 20 December 2009. (b, d, f) Infrared satellite imagery from University of Wisconsin − CIMSS (http://tropic.ssec.wisc.edu/archive/) for (b) 0000 UTC 19 December, (d) 1800 UTC 19 December, and (f) 1200 UTC 20 December 2009. The yellow box denotes the source region for the trajectories shown in Figure 8.

layer that contains the subtropical jet. Particularly telling is the depth of that layer on the anticyclonic shear side of the jet, where positive perturbation depths correspond to excess mass, relative to a long-term mean, residing in the layer. The perturbation pressure depths of various isentropic layers are calculated as the difference between instantaneous pressure depths and a 31-year (1979−2009) average depth at that analysis time for each individual grid point, determined using NCEP's Climate Forecast System Reanalysis (CFSR) dataset (Saha *et al.*, 2010). For the subtropical jet, we consider the pressure depth of the 340−355 K isentropic layer.

The outflow from tropical convection serves as one mechanism through which an isentropic layer can become anomalously inflated. Specifically, tropical convection often ingests boundary layer air with very high equivalent potential temperature (θ_e). Parcels embedded within convective updrafts are then exhausted at an isentropic level that roughly corresponds to this boundary-layer θ_e. Often, such air is within the range of 340−355 K, coinciding with the isentropic layer that houses the subtropical jet. Furthermore, regions characterized by a strong horizontal gradient in perturbation pressure depth are associated with a

perturbation geostrophic vertical shear, in accordance with the isentropic thermal wind relationship:

$$\frac{\partial \overrightarrow{\mathbf{v_g}}'}{\partial \theta} = \frac{1}{\rho f \theta} \mathbf{k} \times \nabla p'. \qquad (2)$$

Consequently, a subtropical jet is typically positioned on the poleward edge of an area characterized by positive perturbation pressure depths in the 340−355 K isentropic layer.

Figure 6(a) demonstrates that at 0000 UTC 19 December, positive perturbation pressure depths in the 340−355 K isentropic layer were found over much of the Gulf of Mexico and Caribbean Sea on the anticyclonic shear side of the subtropical jet. Immediately upstream of the inflated isentropic layer were active areas of organized tropical convection over portions of the eastern equatorial Pacific Ocean and Central America (Figure 6(b)), suggesting that convective outflow was a source of the excess mass found within the isentropic layer. Furthermore, the presence of weak, poleward-directed divergent winds at 200 hPa in the vicinity of the subtropical jet axis (red dashed line) induced a strip of negative PV advection within the 1−3-PVU channel along

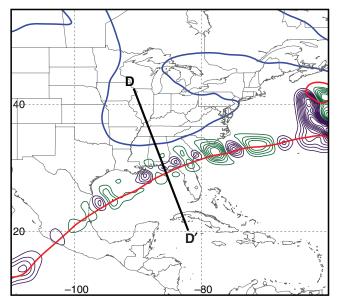**Figure 7.** The 200 hPa positive (negative) PV advection within the 1–3 PVU channel by the total wind contoured in purple (green) every 2×10^{-5} PVU s^{-1} and the 2-PVU surface at 300 hPa (200 hPa) contoured in blue (red), which corresponds to the location of the polar (subtropical) tropopause break, at 1800 UTC 19 December 2009.

the subtropical tropopause break.[††] This negative PV advection suggested a poleward shift in the location of the subtropical jet axis, consistent with the observations made from Figure 5(a,c).

At 1800 UTC 19 December, perturbation pressure depths increased in both magnitude and areal coverage over a large portion of the central Caribbean and off the southeastern United States coast downstream of continued convection in the Tropics (Figure 6(c,d)). An inflation of the $340-355$ K isentropic layer at this time is also apparent on the equatorward side of the subtropical jet within the cross-section D-D′ in Figure 5(d). Figure 6(c) indicates that weak, poleward-directed divergent winds continued to drive a well-defined strip of negative PV advection along the subtropical tropopause break, maintaining support for a poleward shift of the subtropical jet axis. Figure 7, however, depicts the total PV advection at 200 hPa accomplished by the full wind at this time, which indicates only localized regions of weak negative PV advection along the subtropical tropopause break over the Gulf of Mexico. This demonstrates that a large fraction of the negative PV advection accomplished by the divergent wind in Figure 6(c) is mitigated by positive PV advection that must be associated with the non-divergent component of the flow in this location. Consequently, the role of the divergent wind appears to be slight, promoting only a meagre poleward shift in the location of the subtropical jet. Figure 6(e) demonstrates that a subtle poleward shift in the location of the subtropical jet continued up until 1200 UTC 20 December when the polar and subtropical jets superposed. Furthermore, coincident with the superposed jet's increased wind speed at this time is a strengthened gradient in perturbation pressure depth immediately equatorward of the jet axis from the eastern Gulf of Mexico northeastward towards Bermuda.

The upper-tropospheric evolution in the hours preceding superposition strongly suggests that persistent remote tropical convection over the eastern equatorial Pacific Ocean and Central America was responsible for an inflation of the $340-355$ K isentropic layer. An analysis of backward trajectories, using the National Oceanic and Atmospheric Administration
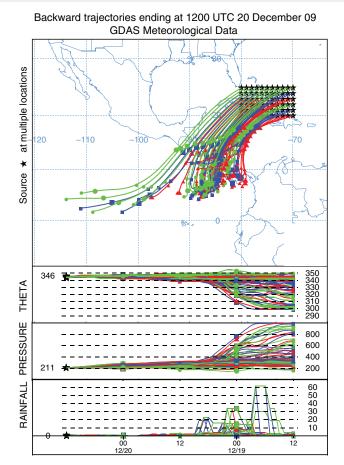

Figure 8. The 48 h backward trajectories initialized at 1200 UTC 20 December 2009 every 1° latitude/longitude within the yellow box (20°N–25°N; 80°W–70°W) shown in Figure 6(e). Trajectories were initialized at 12 000 m above ground level within the NOAA/ARL HYSPLIT model and projected backward using archived NCEP Global Data Assimilation System (GDAS) data and model vertical motion. The GDAS data have a horizontal resolution of $1.0° \times 1.0°$, are interpolated from 23 sigma levels to the mandatory pressure levels, and have a temporal resolution of 3 h. The bottom panels depict the potential temperature (K), pressure (hPa), and rainfall rate (mm h^{-1}) along the path of the trajectories throughout the duration of the simulation.

/Air Resources Laboratory Hybrid Single Particle Lagrangian Integrated Trajectory (NOAA/ARL HYSPLIT) model (Draxler and Hess, 1997, 1998; Draxler, 1999; Draxler and Rolph, 2015; Rolph, 2015), for parcels originating at the centre of the positive pressure perturbation at 1200 UTC 20 December (Figure 8; see figure caption for more details on trajectory calculations) confirms this assertion. Specifically, Figure 8 shows that roughly a fifth of the trajectories are characterized by rapid ascent around 0000 UTC 19 December in the vicinity of the tropical convection shown in Figure 6(b) and warming to potential temperatures of $340-350$ K. Furthermore, rainfall rates along the trajectories strongly suggest that the observed warming and ascent of air parcels is tied to the presence of tropical convection. Upper-tropospheric southwesterly flow downstream of a low-latitude trough west of Mexico, which is identified by the cyclonic curvature of a few trajectories that initiate between 100 and 110°W, subsequently acted to transport the convective outflow towards the Caribbean Sea in the $24-36$ h prior to superposition, resulting in the positive perturbation pressure depths observed there. Forward trajectories (not shown) initiated at the centre of the pressure perturbation at 1200 UTC 20 December show that parcels conserved their potential temperature in the 72 h following jet superposition, as well, indicating little flow out of the $340-355$ K isentropic layer. Consequently, there is strong evidence that the combination of both persistent tropical convection and the approach of a low-latitude trough contributed to the existence and maintenance of a subtropical jet over the Gulf of Mexico: first, by facilitating an inflation of the $340-355$ K isentropic layer in the Tropics and, secondly, by the subsequent

---

[††]The 200 hPa level in this case, as well as in the 2010 Nashville Flood, corresponds well to the level of maximum wind for the subtropical jet and cuts perpendicularly through the subtropical tropopause break (e.g. 2-PVU surface), allowing it to be a suitable level to assess the horizontal advection of the tropopause break by the divergent wind (e.g. Archambault *et al.*, 2013, 2015).
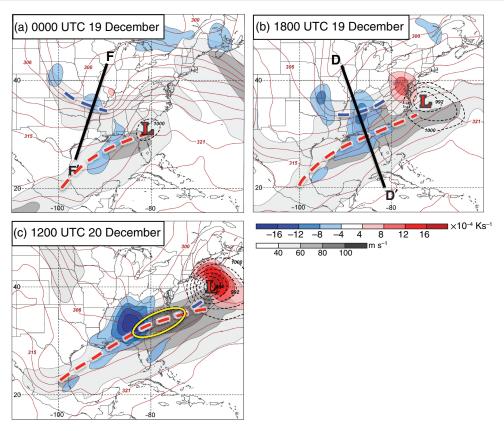
Figure 9. The 250 hPa geostrophic wind speed is shaded with the grey fill pattern according to the legend, 300 hPa geostrophic cold (warm) air advection is shaded in the blue (red) fill pattern following the legend, 500 hPa potential temperature is contoured in red every 3 K, and sea-level pressure is contoured with the dashed black lines every 4 hPa below 1000 hPa for (a) 0000 UTC 19 December, (b) 1800 UTC 19 December, and (c) 1200 UTC 20 December 2009. The polar (subtropical) jet axis is indicated by the thick, dashed blue (red) line, as in Figure 5, the yellow circle highlights the region of jet superposition, and the red 'L' marks the location of the sea-level pressure minimum.

translation of mass within that layer towards higher latitudes where it manifested itself as a positive pressure perturbation and was associated with an increase in westerly vertical shear on its poleward flank.

3.2.2. Polar jet evolution

Focusing attention on the evolution of the polar jet, and its interaction with the subtropical jet, Figure 9(a) shows that the polar jet sat atop a region of enhanced baroclinicity that extended from northwestern Kansas southeastward into northern Mississippi at 0000 UTC 19 December. Furthermore, the geostrophic jet exit region was characterized by weak geostrophic cold air advection over southern Missouri and northern Arkansas. These circumstances support a poleward shift in the jet exit region's ageostrophic transverse circulation so as to position descent through the jet core (Figure 4(b)). The solution for the transverse circulation within the cross-section identified in Figure 9(a) confirms this notion, depicting a region of subsidence centred squarely beneath the polar jet core (Figure 10(a)). A comparison of Figure 10(a) with the total GFS model vertical motion shown in Figure 10(b) indicates a strong agreement between the model vertical motion and the distribution of subsidence associated with the transverse circulation. The subsidence driven by the transverse circulation was specifically tied to the presence of dipole circulations, which consisted of a thermally direct (indirect) circulation to the south (north) of the jet core. This subsidence was not only responsible for strengthening the mid-tropospheric temperature gradient via tilting, but also for supporting a downward protrusion of high-PV air associated with the development of the polar tropopause fold, as denoted by the strip of positive PV advection driven by the circulation in the vicinity of the fold.

By 1800 UTC 19 December, the polar jet had propagated around the base of the polar trough and assumed an orientation

parallel to the axis of the subtropical jet over the southeastern United States (Figure 9(b)). Furthermore, geostrophic wind speeds associated with the polar jet increased to greater than $60 \, \mathrm{m \, s^{-1}}$, in response to the intensified horizontal baroclinicity situated beneath the jet. The magnitude of the geostrophic cold air advection also continued to strengthen in the vicinity of both jets' entrance regions over northern Alabama, implying continued subsidence in the vicinity of the jet cores.

The Sawyer–Eliassen circulation within the cross-section D-D′, drawn through the entrance region of both the polar and subtropical jets at this time, is characterized by a strong thermally direct circulation with subsidence confirmed directly on and beneath the subtropical tropopause step[‡‡] (Figure 10(c)). It is likely that the strength of the circulation arises from its proximity to the weakly stratified, tropical air mass located equatorward of the subtropical jet (e.g. Lang and Martin, 2013). The subsidence associated with the circulation also accounted for the large majority of the positive PV advection diagnosed along the subtropical tropopause step in Figure 10(c) (not shown). Once again, the distribution of subsidence compared well with the model vertical motion in Figure 10(d), which was also characterized by a maximum in subsidence beneath the subtropical tropopause step that tilted equatorward with increasing elevation. Consequently, it can be concluded that the diagnosed subsidence was favourably positioned to advect high-PV air downward and to lower the altitude of the subtropical tropopause step with time.

From another perspective, it is apparent that the 320 and 325 K isentropes were situated within the horizontal baroclinicity that sat beneath the subtropical jet. The presence of a mid-tropospheric maximum in subsidence through the polar jet core,

---

[‡‡]Cross-sections along the entire length of the polar and subtropical jets at this time are consistent with the result shown in Figure 10(c).
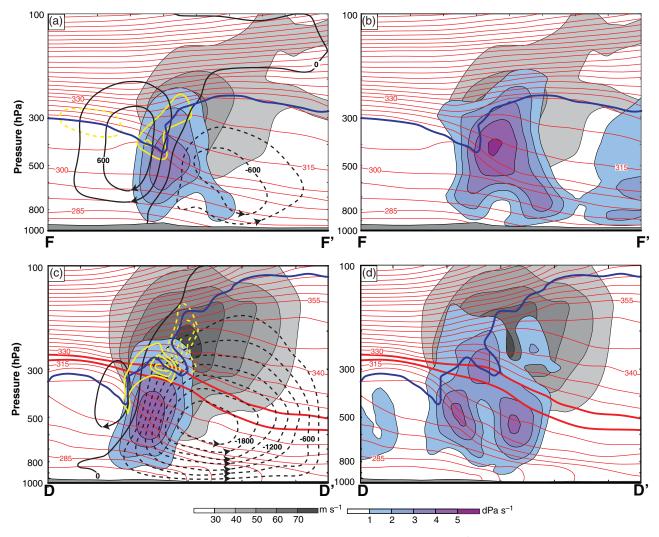
Figure 10. (a, c) Cross-sections, as indicated in Figure 9, of Sawyer–Eliassen stream function every 300 m hPa s^{-1} with negative (positive) values contoured with dashed (solid) black lines, potential temperature every 5 K contoured in red, positive omega associated with the Sawyer–Eliassen circulation shaded in the purple fill pattern following the legend, geostrophic wind speeds shaded with the grey fill pattern according to the legend, positive (negative) PV advection within the 1–3-PVU channel by the Sawyer–Eliassen circulation contoured with the solid (dashed) yellow lines every 2×10^{-5} PVU s^{-1}, and the 1.5-PVU surface identified by the bold blue line. The sense of the circulation is depicted by the arrowheads plotted on the stream function contours. The 320 and 325 K isentropes are made bold in (c) for reasons discussed in the text. (b,d) Wind speed, PV and potential temperature distributions are identical to those in (a,c) with subsidence from the GFS analysis now shaded in the purple fill pattern.

as indicated in Figure 10(c), implies that the 320 K isentrope was advected downward on the poleward side of the subtropical jet at a more rapid rate than the 325 K isentrope, reducing the horizontal baroclinicity beneath the subtropical jet. At the same time, the subsidence acted to incorporate these same isentropes into a strengthening region of baroclinicity beneath the polar jet core (Figure 5(f)). Consequently, the subsidence associated with the Sawyer–Eliassen circulation promoted an intensification of the baroclinicity directly beneath the polar jet core at the expense of the subtropical jet's baroclinicity and, subsequently, the production of one consolidated region of intense horizontal temperature contrast that is characteristic of a superposed jet.

Also of note is the potential role that the upper-level branch of the transverse circulation may have played in horizontally displacing the subtropical tropopause break. Figure 10(c) indicates a region of negative PV advection that was centred squarely along the subtropical tropopause break and that was primarily attributable to the upper-level branch of the circulation (not shown). The magnitude of this negative PV advection also compares well with the negative PV advection by the full divergent wind at 200 hPa in Figure 6(c). However, given that the total horizontal PV advection along the subtropical tropopause break was found to be small (Figure 7), it can be concluded that the influence of the upper-level branch of the circulation on restructuring the tropopause was relatively minimal compared to the circulation's subsiding branch.

By 1200 UTC 20 December, the polar tropopause break became vertically aligned with the subtropical tropopause break, producing the vertical PV wall shown in Figure 5(f) and a superposed jet from central Georgia northeastward to eastern North Carolina (Figure 9(c)). Wind speeds in the core of the superposed jet increased as well, consistent with the consolidation of baroclinicity beneath the superposed jet.

3.2.3. Synthesis

The preceding analysis of this case is summarized in the conceptual diagram shown in Figure 11, which highlights the importance of internal jet dynamics for facilitating a vertical superposition of the polar and subtropical jets. While remote convection over Central America and the equatorial Pacific Ocean was essential for strengthening and establishing the subtropical jet over the Gulf of Mexico, the upper-tropospheric divergent wind only promoted a slight poleward shift in the location of the subtropical jet axis in that location. Ageostrophic transverse circulations, on the other hand, were crucial in their ability to restructure the tropopause into the two-step structure characteristic of a superposition. Specifically, the subsiding branches of these circulations were not only favourably positioned to support the production of a polar tropopause fold, but also to drive a downward protrusion of high-PV air that was centred squarely on and beneath the subtropical tropopause step. Consequently, this
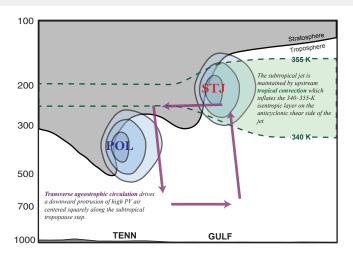
Figure 11. Conceptual diagram (distance/pressure in hPa) summarizing the development of a superposed jet during the 18–20 December 2009 Mid-Atlantic Blizzard. 'TENN' corresponds to Tennessee and 'GULF' denotes the location of the Gulf Coast.

subsidence, which was present throughout the 18 h period prior to superposition (not shown), was found to lower the tropopause height between the polar and subtropical jets and to consolidate the baroclinicity associated with each jet into a single zone of horizontal temperature contrast.

4. Jet evolution during the 1–3 May 2010 Nashville Flood

4.1. Synoptic overview

As described by WM14, the 1–3 May 2010 Nashville Flood was an historic two-day event in which two consecutive mesoscale convective systems (MCSs) were responsible for rainfall accumulations in excess of 180 mm (7 in) across a large portion of Tennessee, southern Kentucky, and northern Mississippi (Moore *et al.*, 2012, their Fig. 1). Moore *et al.* (2012) and Durkee *et al.* (2012) provide excellent overviews of both the meso- and synoptic-scale processes responsible for the production of precipitation in this case and the reader is referred to those works for any additional information. As with the December 2009 case, here we present an abbreviated synoptic overview that focuses solely on the jet evolution in the upper troposphere during the 24 h period of 0000 UTC 1 May to 0000 UTC 2 May 2010 across the contiguous United States.

Figure 12(a) depicts a high-amplitude flow pattern in place over a large portion of North America at 0000 UTC 1 May, with a deep, positively tilted trough over the western United States and a strong ridge over the east. A polar jet was identified downstream of the trough axis and extended from Baja California northeastward into the Central Plains, while a subtropical jet, which was of comparable strength to the polar jet, stretched from northern Mexico eastward along the Gulf Coast. Note that at this time, even though the two jets are in close proximity to one another, they are not superposed. A cross-section through the two separate jet cores (Figure 12(b)) confirms this diagnosis and depicts a clear, three-step tropopause structure with each tropopause break associated with a distinct wind speed maximum.

At 1200 UTC 1 May, a broad area of precipitation situated over much of the Ohio River Valley helped to further build the extensive ridge that was in place over a large portion of the eastern United States via a diabatic erosion of upper-tropospheric PV. This is best illustrated by a substantial poleward retreat in the location of the 2-PVU contour at 200 hPa over the eastern United States in Figure 15. Consequently, in response to the strengthened ridge, the axis of the subtropical jet shifted noticeably poleward and westward, bringing it closer to the polar jet (Figure 12(c)). A cross-section through the two jet structures at this time illustrates that a three-step tropopause structure remained intact, while

clearly showing the movement of the subtropical jet towards the northwest and a wind speed increase in both jets (Figure 12(d)).

At 0000 UTC 2 May, the polar and subtropical jets became superposed over portions of west Texas and southwestern Oklahoma, as the axis of the subtropical jet continued to migrate towards the northwest and the western trough shifted slowly eastward (Figure 12(e)). A cross-section through the superposed portion of the jet (Figure 12(f)) shows both the appearance of a slight equatorward shift in the location of the polar tropopause break within the plane of the cross-section and the continued northwestward migration of the subtropical tropopause break, which combined to produce the two-step tropopause structure and vertical PV wall characteristic of a superposition. Further note that the two wind speed maxima are now consolidated into a single jet core that featured wind speeds greater than 70 m s^{-1} in response to the increased horizontal baroclinicity in the upper troposphere and lower stratosphere that accompanied the superposition (Figure 12(f)).

4.2. Superposed jet formation

4.2.1. Polar jet evolution

At 0000 UTC 1 May, the polar jet sat atop a rather extensive and continuous area of mid-tropospheric baroclinicity that stretched from just off the coast of southern California into northern Minnesota, as indicated by the 400 hPa temperature analysis in Figure 13(a). Furthermore, the entrance region of the polar jet was characterized by an area of geostrophic cold air advection centred squarely in the base of the western trough. This circumstance promotes subsidence beneath the jet core (Shapiro, 1982) by shifting the thermally direct circulation in the entrance region towards the anticyclonic shear side of the jet (Figure 4(b)).

The Sawyer–Eliassen circulation within the cross-section identified in Figure 13(a) illustrates the presence of subsidence directly beneath the polar jet core and in the vicinity of the polar tropopause fold (Figure 14(a)). As for the circulations diagnosed in the previous case, the spatial distribution of the subsidence associated with the transverse circulation in Figure 14(a) matches well with the distribution of model vertical motion shown in Figure 14(b). However, it is notable that the subsidence in Figure 14(a) is substantially weaker in magnitude and more spatially confined than its model vertical motion counterpart. Nevertheless, the diagnosed subsidence, once again, promotes a downward protrusion of high-PV air into the middle troposphere, as denoted by the positive PV advection situated in the polar tropopause fold (Figure 14(a)), while simultaneously acting to increase the horizontal baroclinicity beneath the jet via tilting. Subsequently, regions of strong mid-tropospheric baroclinicity in the base of the trough correspond roughly to the location of the polar tropopause fold in Figure 13.

It is also likely that the strong curvature associated with the western trough further enhanced the total subsidence observed in the jet entrance region beyond that estimated by the transverse circulation, given the differences between Figure 14(a) and (b). Specifically, Figure 15 indicates that an easterly divergent wind characterized the base of the trough during the 24 h that preceded superposition, consistent with the expectation of subgeostrophic flow through a trough. Furthermore, Figure 15 indicated a maximum in velocity potential that was persistently located upstream of the trough axis. Local maxima (minima) in velocity potential in the upper troposphere correspond to convergence (divergence) aloft [$\nabla^2 \chi = \partial u_{\mathrm{div}}/\partial x + \partial v_{\mathrm{div}}/\partial y$, where $\nabla \chi = \overrightarrow{v_{\mathrm{div}}}$] and descent (ascent) in the column below via continuity. Consequently, a portion of the divergent wind field is a result of flow curvature, which accentuated both the subsidence observed upstream of the trough axis and the development of the polar tropopause fold.

At 1200 UTC 1 May, the axis of the polar jet became fractured near the United States/Mexico border (Figure 13(b)), partially
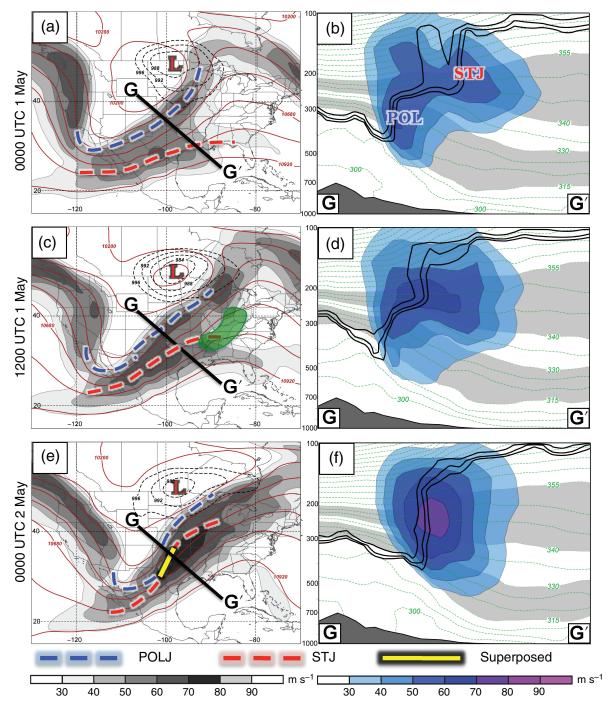
Figure 12. Conventions are identical to Figure 5 but for (a,b) 0000 UTC 1 May, (c,d) 1200 UTC 1 May, and (e,f) 0000 UTC 2 May 2010. The precipitation shield at 1200 UTC 1 May 2010 in (c) is denoted by the green shading and sea-level pressure is now contoured every 4 hPa below 996 hPa in (a, c, e).

due to the influence of ongoing convection over the southern Mississippi River Valley and an associated region of negative PV advection along the polar tropopause break driven by the divergent wind (not shown). Additionally, locations between the polar and subtropical jet axes over the Southern Plains (Figure 12(c)) were characterized by an environment favourable for large-scale ascent (refer to the minimum in velocity potential located immediately downstream of the trough in Figure 15(b)), given both the close proximity of the upstream trough and a region of geostrophic warm air advection along the polar jet axis (Figure 13(b)). This large-scale ascent was responsible for decreasing the horizontal temperature gradient in the middle troposphere via tilting downstream of the Rio Grande, as demonstrated by the weakened 400 hPa temperature gradient in that area compared to locations further upstream (Figure 13(b)). However, while not explicitly shown, the diagnosed ascent over the Southern Plains at this time did not play an important role in the development of a superposition, as the ascent was not associated with any substantial latent heat release that would

restructure the tropopause via an erosion of upper-tropospheric PV (ongoing heavy precipitation identified in Figure 12(c) was displaced well to the east) and the strong static stability above the subtropical tropopause step (refer to Figure 12(d)) was found to deter any substantial upward movement of the tropopause by vertical advection. Farther upstream, in the base of the trough, geostrophic jet wind speeds increased from the previous time in response to the strengthened baroclinicity beneath the polar jet. Geostrophic cold air advection remained strong in the base of the trough at this time as well, suggesting continued subsidence in the vicinity of the polar jet core and the subsequent maintenance of the polar tropopause fold and mid-tropospheric baroclinicity.

At 0000 UTC 2 May, the polar jet streak in the base of the trough was positioned slightly downstream of its previous location, such that its most downstream edge overlapped with the region of superposition identified in Figure 12(e) over southwestern Oklahoma and west Texas (Figure 13(c)). Furthermore, rather intense baroclinicity, which extended from the Southern Plains upstream to Baja California, continued to characterize the polar jet
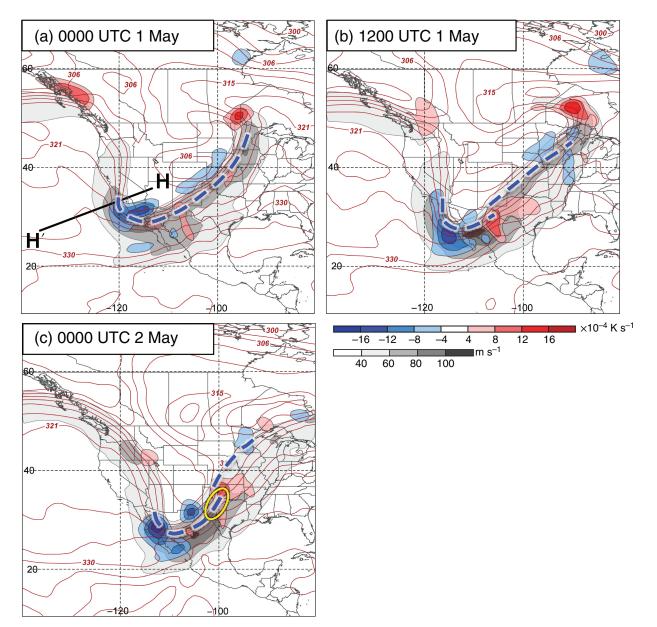
Figure 13. The 300 hPa geostrophic wind speed is shaded in the grey fill pattern according to the legend, 300 hPa geostrophic cold (warm) air advection is shaded in the blue (red) fill pattern following the legend, and 400 hPa potential temperature is contoured in red every 3 K at (a) 0000 UTC 1 May, (b) 1200 UTC 1 May, and (c) 0000 UTC 2 May 2010. Polar jet axes from Figure 12 are indicated by the thick, blue dashed lines and the yellow circle highlights the region of jet superposition.
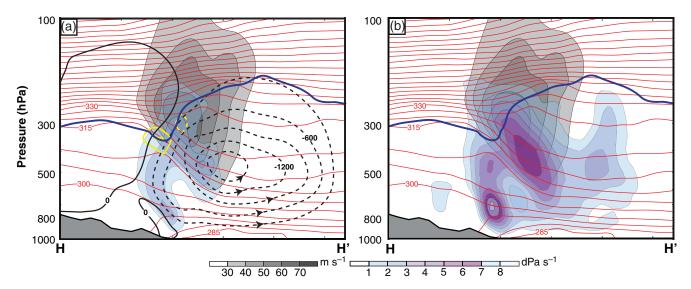

Figure 14. (a, b) Conventions are identical to those in Figure 10, but for the cross-section H-H′ shown in Figure 13(a).
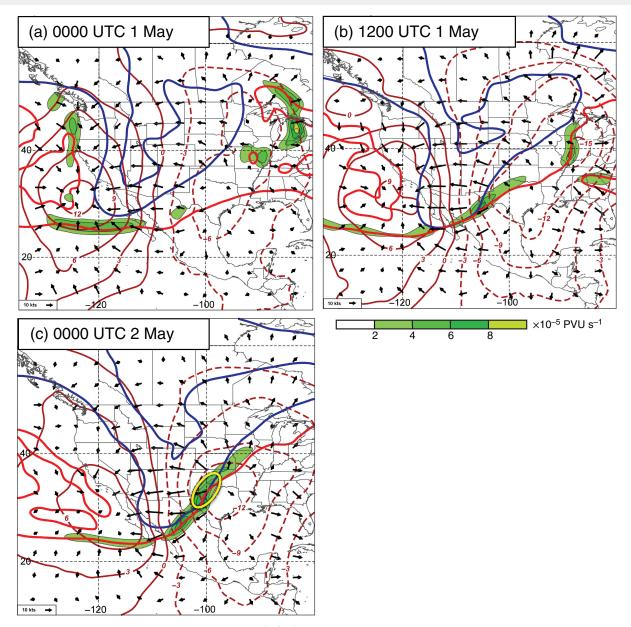
Figure 15. The 200 hPa velocity potential is contoured every $3 \times 10^6 \, \text{m}^2 \, \text{s}^{-1}$ with positive (negative) values identified with solid (dashed) thick dark red lines, the 2-PVU contour at 300 hPa (200 hPa) is identified with the thick blue (red) line, and negative PV advection within the 1−3-PVU channel by the divergent wind (arrows) at 200 hPa is shaded in the green fill pattern following the legend, at (a) 0000 UTC 1 May, (b) 1200 UTC 1 May, and (c) 0000 UTC 2 May 2010.

stream. Recalling that this area of baroclinicity was also associated with the development of a polar tropopause fold, it becomes clear that the appearance of an equatorward displacement of the polar tropopause break within Figure 12(d,f) is simply the downstream propagation of an intense polar tropopause fold into the area of superposition, as the trough slowly migrated eastward.

4.2.2. Subtropical jet evolution

As suggested, the evolution of the subtropical jet is closely tied to the persistent convection present over portions of the southern Mississippi River Valley throughout the duration of the flooding event. Recall that at 0000 UTC 1 May the subtropical jet was characterized by a rather zonal orientation and was distinct from the polar jet (Figure 12(a)). Furthermore, Figure 15(a) depicts an elongated minimum in velocity potential at 200 hPa (approximately the level of maximum divergent outflow) centred over the Mississippi River Valley, consistent with the presence of large-scale ascent in that location, and a maximum in velocity potential immediately upstream of the trough over the western United States. The juxtaposition of these two features resulted in the presence of easterly divergent winds over the spine of the Rocky Mountains and northern Mexico. At this time, these divergent winds were responsible for only a weak region of negative PV

advection over northern Mexico along the subtropical tropopause break, given its rather zonal orientation.

By 1200 UTC 1 May, it is apparent that latent heating from the ongoing convection over the southern Mississippi River Valley (see Figure 12(c)) had resulted in a substantial diabatic erosion of upper-tropospheric PV in that location, as demonstrated by the poleward retreat of the 2-PVU contour at 200 hPa (Figure 15(b)). Consequently, the subtropical jet became characterized predominantly by southwesterly flow and took on an orientation that was roughly parallel to the polar jet. Divergent winds across northern Mexico also strengthened considerably over the previous 12 h, largely due to the enhanced outflow from convection over portions of Tennessee and southern Kentucky. The combination of these two factors resulted in a significantly more favourable situation for the divergent wind to displace the subtropical tropopause break towards the northwest, as indicated by the increase in negative PV advection along the subtropical tropopause break.

The influence of the divergent wind is best analysed in the context of Figure 16, which shows the total PV advection accomplished at 200 hPa at this time along the subtropical tropopause break. From this analysis, it is evident that the divergent wind slows the eastward translation of the subtropical tropopause break over northern Mexico, given the strip of positive
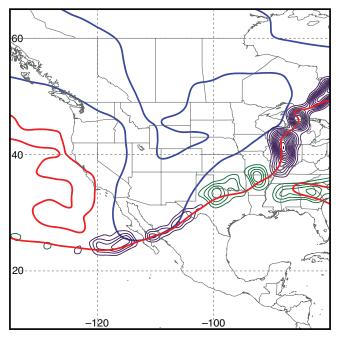
Figure 16. Conventions are identical to those in Figure 7, but at 1200 UTC 1 May 2010.

Figure 17. Conceptual diagram (distance/pressure in hPa) summarizing the development of a superposed jet during the 1–3 May 2010 Nashville Flood. 'OKLA' corresponds to Oklahoma and 'GULF' denotes the location of the Gulf Coast.

PV advection found in that location in Figure 16. This mechanism, whereby the divergent wind slows the eastward progression of a midlatitude trough, is similar to that identified by Archambault *et al.* (2015), among others, in cases of ET. Over Texas and Oklahoma, the divergent and non-divergent wind fields appear to combine constructively to drive a region of negative PV advection. Consequently, the northwestward shift in the position of the subtropical jet axis over the Southern Plains is aided by the convective outflow and continued up until 0000 UTC 2 May, when the subtropical jet became vertically superposed with the polar jet over portions of west Texas and southwestern Oklahoma (Figure 15(c)).

4.2.3.   Synthesis

In contrast to the December 2009 case, jet superposition in the May 2010 case was more strongly dependent on the presence of convection over the southeastern United States. The analysis, which is summarized in Figure 17, demonstrates that the convection acted to substantially restructure the tropopause via (i) the diabatic erosion of upper-tropospheric PV, and (ii) advection of the subtropical jet axis westward towards the polar jet via its associated divergent outflow. This result aligns particularly well with existing evidence illustrating the role that tropopause-level outflow can play in influencing the strength and location of a particular jet stream (e.g. Grams *et al.*, 2011, 2013; Archambault *et al.*, 2013, 2015). However, in contrast to the December 2009 case, ageostrophic transverse circulations played a more indirect role in the production of a superposition during the 2010 Nashville Flood. Specifically, persistent geostrophic cold air advection in the base of the western trough was responsible for driving an area of subsidence in the vicinity of the polar jet core that facilitated the development of a polar tropopause fold. This fold subsequently propagated downstream into west Texas and southwestern Oklahoma by 0000 UTC 2 May where it undercut the retreating subtropical tropopause break, thereby facilitating the development of the superposed jet structure.

5.   Discussion

Motivated by the identification of jet superpositions in several historic and recent high-impact sensible weather events, this study examines the dynamical processes responsible for producing a superposition during the 18–20 December 2009 Mid-Atlantic
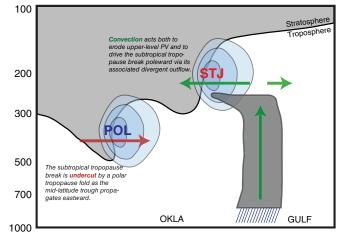
Blizzard and the 1–3 May 2010 Nashville Flood. The two cases selected highlight the fact that jet superpositions can be associated with different types of high-impact weather events and can develop at different times of year. Given that ageostrophic transverse jet circulations and convection both influence the restructuring of the tropopause within single-jet environments, the analysis focuses on the role these same mechanisms play in reshaping the tropopause within the more complex double-jet environment.

Both cases were characterized by mid-tropospheric geostrophic cold air advection in cyclonic shear along a portion of the polar jet at some point prior to superposition, indicating that subsidence was positioned directly through and beneath the polar jet core. Consequently, the descending motions were favourably positioned to facilitate downward advection of high-PV air from the stratosphere and contribute to the requisite restructuring of the tropopause that characterizes a jet superposition. In the December 2009 case, this subsidence was specifically positioned directly on and beneath the subtropical tropopause step and in the immediate vicinity of both the polar and subtropical jets. Consequently, subsidence played a primary role in the production of a superposition by lowering the tropopause height in the region between the two individual jets and by consolidating the baroclinicity associated with each jet into one single zone of contrast. For comparison, only the jet entrance region of the polar jet was characterized by subsidence during the May 2010 Flood, as locations in close proximity to the jet superposition over the Southern Plains were characterized by geostrophic warm air advection and large-scale ascent. However, the large-scale ascent did not play a substantial role in the production of a superposition, as the ascent was positioned between the two jet cores, was not associated with any appreciable latent heating that would erode upper-tropospheric PV, and was incapable of facilitating a substantial vertical displacement of the subtropical tropopause step given the strong static stability within the lower stratosphere. Consequently, vertical motions in the May 2010 case were only found to foster the development of a polar tropopause fold, instead of working to directly assimilate the two jets into a single structure.

The two cases examined as part of this study also demonstrate the different roles that convection can play in facilitating a superposition. For instance, during the May 2010 Flood, convection occurred in the immediate vicinity of the subtropical jet on its equatorward flank. This convection subsequently acted to restructure the tropopause via material displacement and diabatic erosion of upper-tropospheric PV and served as a primary mechanism supporting superposition in that case. Conversely, the December 2009 case was associated with remote convection that occurred in the Tropics. This tropical convection was primarily

responsible for substantially enhancing and maintaining the strength of the subtropical jet by inflating the anticyclonic shear side of the isentropic layer containing the jet. Together, these two cases demonstrate that the proximity of convection to the jet structure can determine the nature of its influence on the jet. For example, proximate convection can have a locally intense but temporally transient impact on the jet structure through its divergent outflow and latent heat release. Alternatively, remote convection can drive a slower-acting, but persistent impact via the development of what might be termed tropical tropopause anticyclones – the balanced response to upper-tropospheric mass deposition on the anticyclonic shear side of the subtropical jet.

While both cases illustrate that internal jet dynamics and convection can play important roles in the development of a superposition, it is clear that the individual importance of each component to the process of jet superposition depends on the case being considered. For instance, it appears that internal jet dynamics played a more prominent role during the December 2009 case, while convection was the dominant component during the May 2010 Flood. Given that these are only two cases, a broader survey of jet superposition events over North America may help (i) to pinpoint the variety of environmental characteristics that are most conducive for the development of superpositions, and (ii) to determine whether or not that preferred environment varies seasonally or geographically.

Finally, persistent observation of these structures by the authors throughout the development of this study has made clear that significant weather is not tied to every jet superposition event. Consequently, greater knowledge regarding the environmental differences that exist between null cases and those associated with significant high-impact weather over North America remains outstanding. Ultimately, the ability to diagnose the formation of these structures, and to understand the circumstances that permit them to contribute to the production of high-impact weather at middle latitudes, could have important implications for short-term weather prediction.

Acknowledgements

References

Agusti-Panareda A, Thorncroft CD, Craig GC, Gray SL. 2004. The extratropical transition of Hurricane *Irene* (1999): A potential-vorticity perspective. *Q. J. R. Meteorol. Soc.* **130**: 1047–1074.

Ahmadi-Givi F, Graig GC, Plant RS. 2004. The dynamics of a midlatitude cyclone with very strong latent-heat release. *Q. J. R. Meteorol. Soc.* **130**: 295–323.

Archambault HM, Bosart LF, Keyser D, Cordeira JM. 2013. A climatological analysis of the extratropical flow response to recurving western North Pacific tropical cyclones. *Mon. Weather Rev.* **141**: 2325–2346.

Archambault HM, Keyser D, Bosart LF, Davis CA, Cordeira JM. 2015. A composite perspective of the extratropical flow response to recurving western North Pacific tropical cyclones. *Mon. Weather Rev.* **143**: 1122–1141.

Bosart LF, Hakim GJ, Tyle KR, Bedrick MA, Bracken WE, Dickinson MJ, Schultz DM. 1996. Large-scale antecedent conditions associated with the 12–14 March 1993 cyclone ('Superstorm '93') over eastern North America. *Mon. Weather Rev.* **124**: 1865–1891.

Christenson CE. 2013. 'A synoptic-climatology of Northern Hemisphere polar and subtropical jet superposition events'. MS thesis, Department of Atmospheric and Oceanic Sciences, University of Wisconsin-Madison, WI.

Christenson CE, Martin JE. 2012. 'The large-scale environment associated with the 25–28 April 2011 severe weather outbreak.' In *16th NWA Severe Storms and Doppler Radar Conference*, 31 March 2012. Des Moines, IA, National Weather Association: Norman, OK.

Davis CA, Emanuel KE. 1991. Potential vorticity diagnostics of cyclogenesis. *Mon. Weather Rev.* **119**: 1929–1953.

Dean DB, Bosart LF. 1996. Northern Hemisphere 500-hPa trough merger and fracture: a climatology and case study. *Mon. Weather Rev.* **124**: 2644–2671.

Defant F. 1959. On hydrodynamic instability caused by an approach of subtropical and polarfront jet stream in northern latitudes before the onset of strong cyclogenesis. In *The Atmosphere and Sea in Motion*, Bolin B. (ed.).: 305–325. Rockefeller and Oxford University Press: New York, NY.

Defant F, Taba H. 1957. The threefold structure of the atmosphere and the characteristics of the tropopause. *Tellus* **9**: 259–275.

desJardins ML, Brill KF, Schotz SS. 1991. Use of GEMPAK on UNIX workstations. In *Preprints, Seventh International Conference on Interactive Information and Processing Systems for Meteorology, Oceanography, and Hydrology*: 449–453. American Meteorological Society: New Orleans, LA.

Draxler RR. 1999. *HYSPLIT4 User's Guide. NOAA* Technical Memorandum, ERL ARL-230. NOAA Air Resources Laboratory: Silver Spring, MD.

Draxler RR, Hess GD. 1997. *Description of the HYSPLIT_4 Modeling System. NOAA Technical Memorandum* ERL ARL-224. NOAA Air Resources Laboratory: Silver Spring, MD.

Draxler RR, Hess GD. 1998. An overview of the HYSPLIT_4 modeling system of trajectories, dispersion, and deposition. *Aust. Meteorol. Mag.* **47**: 295–308.

Draxler RR, Rolph GD. 2015. *HYSPLIT (Hybrid Single-Particle Lagrangian Integrated Trajectory) Model Access via NOAA ARL READY*. NOAA Air Resources Laboratory: Silver Spring, MD. http://ready.arl.noaa.gov/HYSPLIT.php (accessed 3 November 2015).

Durkee JD, Campbell L, Berry K, Jordan D, Goodrich G, Mahmood R, Foster S. 2012. A synoptic perspective of the record 1–2 May 2010 mid-South heavy precipitation event. *Bull. Am. Meteorol. Soc.* **93**: 611–620.

Eichelberger SJ, Hartmann DL. 2007. Zonal jet structure and the leading mode of variability. *J. Clim.* **20**: 5149–5163.

Eliassen A. 1962. On the vertical circulation in frontal zones. *Goephys. Publ.* **24**: 147–160.

Gaza RS, Bosart LF. 1990. Trough merger characteristics over North America. *Weather and Forecasting* **5**: 314–331.

Grams CM, Wernli H, Böttcher M, Čampa J, Corsmeier U, Jones SC, Keller JH, Lenz C-J, Wiegand L. 2011. The key role of diabatic processes in modifying the upper-tropospheric wave guide: A North Atlantic case-study. *Q. J. R. Meteorol. Soc.* **137**: 2174–2193.

Grams CM, Jones SC, Davis CA, Harr PA, Weissmann M. 2013. The impact of Typhoon *Jangmi* (2008) on the midlatitude flow. Part I: Upper-level ridgebuilding and modification of the jet. *Q. J. R. Meteorol. Soc.* **139**: 2148–2164.

Griffin KS, Bosart LF. 2014. The extratropical transition of Tropical Cyclone *Edisoana* (1990). *Mon. Weather Rev.* **142**: 2772–2793.

Hakim GJ, Bosart LF, Keyser D. 1995. The Ohio Valley wave-merger cyclogenesis event of 25–26 January 1978. Part I: Multiscale case study. *Mon. Weather Rev.* **123**: 2663–2692.

Hakim GJ, Keyser D, Bosart LF. 1996. The Ohio Valley wave-merger cyclogenesis event of 25–26 January 1978. Part II: Diagnosis using quasigeostrophic potential vorticity inversion. *Mon. Weather Rev.* **124**: 2176–2205.

Harnik N, Galanti E, Martius O, Adam O. 2014. The anomalous merging of the African and North Atlantic jet streams during Northern Hemisphere winter of 2010. *J. Clim.* **27**: 7319–7334.

Hoskins BJ, Berrisford P. 1988. A potential vorticity perspective of the storm of 15–16 October 1987. *Weather* **43**: 122–129.

Keyser D, Shapiro MA. 1986. A review of the structure and dynamics of upper-level frontal zones. *Mon. Weather Rev.* **114**: 452–499.

Koteswaram P. 1953. An analysis of the high tropospheric wind circulation over India in winter. *Indian J. Meteorol. Geophys.* **4**: 13–21.

Koteswaram P, Parthasarathy S. 1954. The mean jet stream over India in the pre-monsoon and post-monsoon seasons and vertical motions associated with sub-tropical jet streams. *Indian J. Meteorol. Geophys.* **5**: 138–156.

Krishnamurti TN. 1961. The subtropical jet stream of winter. *J. Meteorol.* **18**: 172–191.

Lai C-C, Bosart LF. 1988. A case study of trough merger in split westerly flow. *Mon. Weather Rev.* **116**: 1838–1856.

Lang AA, Martin JE. 2012. The structure and evolution of lower stratospheric frontal zones. Part I: Examples in northwesterly and southwesterly flow. *Q. J. R. Meteorol. Soc.* **138**: 1350–1365.

Lang AA, Martin JE. 2013. The structure and evolution of lower stratospheric frontal zones. Part II: The influence of tropospheric convection on lower stratospheric frontal development. *Q. J. R. Meteorol. Soc.* **139**: 1798–1809.

Lee S, Kim H-K. 2003. The dynamical relationship between subtropical and eddy-driven jets. *J. Atmos. Sci.* **60**: 1490–1503.

Loewe F, Radok V. 1950. A meridional aerological cross section in the southwest Pacific. *J. Meteorol.* **7**: 58–65.

McTaggart-Cowan R, Gyakum JR, Yau MK. 2001. Sensitivity testing of extratropical transitions using potential vorticity inversions to modify initial conditions: Hurricane *Earl* case study. *Mon. Weather Rev.* **129**: 1617–1636.

McTaggart-Cowan R, Gyakum JR, Yau MK. 2004. The impact of tropical remnants on extratropical cyclogenesis: Case study of Hurricanes *Danielle* and *Earl* (1998). *Mon. Weather Rev.* **132**: 1933–1951.

McTaggart-Cowan R, Bosart LF, Gyakum JR, Atallah EH. 2007. Hurricane *Katrina* (2005). Part II: Evolution and hemispheric impacts of a diabatically generated warm pool. *Mon. Weather Rev.* **135**: 3927–3949.

Martin JE. 2014. Quasi-geostrophic diagnosis of the influence of vorticity advection on the development of upper level jet-front systems. *Q. J. R. Meteorol. Soc.* **140**: 2658–2671.

Martius O, Schwierz C, Davies HC. 2010. Tropopause-level waveguides. *J. Atmos. Sci.* **67**: 866–879.

Mohri K. 1953. On the fields of wind and temperature over Japan and adjacent waters during winter of 1950–1951. *Tellus* **5**: 340–358.

Moore BJ, Neiman PJ, Ralph FM, Barthold FE. 2012. Physical processes associated with heavy flooding rainfall in Nashville, Tennessee, and vicinity during 1–2 May 2010: The role of an atmospheric river and mesoscale convective systems. *Mon. Weather Rev.* **140**: 358–378.

Morgan MC, Nielsen-Gammon JW. 1998. Using tropopause maps to diagnose midlatitude weather systems. *Mon. Weather Rev.* **126**: 241–265.

Namias J, Clapp PF. 1949. Confluence theory of the high tropospheric jet stream. *J. Meteorol.* **6**: 330–336.

National Weather Service. 2014. 'December 18–19, 2009 winter storm'. http://www4.ncsu.edu/~nwsfo/storage/cases/20091218/ (accessed 23 April 2015).

Newton CW. 1954. Frontogenesis and frontolysis as a three-dimensional process. *J. Meteorol.* **11**: 449–461.

O'Rourke AK, Vallis GK. 2013. Jet interaction and the influence of a minimum phase speed bound on the propagation of eddies. *J. Atmos. Sci.* **70**: 2614–2628.

Palmén E, Newton CW. 1948. A study of the mean wind and temperature distribution in the vicinity of the polar front in winter. *J. Meteorol.* **5**: 220–226.

Palmén E, Newton CW. 1969. *Atmospheric Circulation Systems: Their Structure and Physical Interpretation.* Academic Press: New York, NY.

Riehl H. 1962. 'Jet streams of the atmosphere,' Department of Atmospheric Science Technical Report 32. Colorado State University: Fort Collins, CO.

Rolph GD. 2015. 'Real-time environmental applications and display system (READY)'. NOAA Air Resources Laboratory: Silver Spring, MD. http://ready.arl.noaa.gov (accessed 3 November 2015).

Saha S, Mourthi S, Pan H-L, Wu XR, Wang JD, Nadiga S, Tripp P, Kistler R, Woollen J, Behringer D, Liu HX, Stokes D, Grumbine R, Gayno G, Wang J, Hou Y-T, Chuang H-Y, Juang H-MH, Sela J, Iredell M, Treadon R, Kleist D, Van Delst P, Keyser D, Derber J, Ek M, Meng J, Wei HL, Yang RQ, Lord S, Van Den Dool H, Kumar A, Wang WQ, Long C, Chelliah M, Xue Y, Huang BY, Schemm J-K, Ebisuzaki W, Lin R, Xie PP, Chen MY, Zhou ST, Higgins W, Zou C-Z, Liu QH, Chen Y, Han Y, Cucurull L, Reynolds RW, Rutledge G, Goldberg M. 2010. The NCEP climate forecast system reanalysis. *Bull. Am. Meteorol. Soc.* **91**: 1015–1057.

Sawyer JS. 1956. The vertical circulation at meteorological fronts and its relation to frontogenesis. *Proc. R. Soc. London* **234A**: 346–362.

Shapiro MA. 1982. *Mesoscale Weather Systems of the Central United States.* CIRES, University of Colorado/NOAA: Boulder, CO.

Shapiro MA, Keyser D. 1990. Fronts, jet streams, and the tropopause. In *Extratropical Cyclones: The Erik Palmén Memorial Volume*, Newton C, Holopainen EO. (eds.): 167–191. American Meteorological Society: Boston, MA.

Shapiro MA, Wernli H, Bao J-W, Methven J, Zou X, Doyle J, Holt T, Donall-Grell E, Neiman P. 1999. A planetary-scale to mesoscale perspective of the life cycles of extratropical cyclones: The bridge between theory and observations. In *The Life Cycles of Extratropical Cyclones*, Shapiro M, Grønås S. (eds.): 139–185. American Meteorological Society: Boston, MA.

Son S-W, Lee S. 2005. The response of westerly jets to thermal driving in a primitive equation model. *J. Atmos. Sci.* **62**: 3741–3757.

Strahl JLS, Smith PJ. 2001. A diagnostic study of an explosively developing extratropical cyclone and an associated 500-hPa trough merger. *Mon. Weather Rev.* **129**: 2310–2328.

Sutcliffe RC. 1947. A contribution to the problem of development. *Q. J. R. Meteorol. Soc.* **73**: 370–383.

Sutcliffe RC, Bannon JK. 1954. Seasonal changes in the upper-air conditions in the Mediterranean Middle East area. In *Proceedings of International Association of Meteorology*: 322–334. International Union of Geodesy and Geophysics: Rome.

Winters AC, Martin JE. 2014. The role of a polar/subtropical jet superposition in the May 2010 Nashville Flood. *Weather and Forecasting* **29**: 954–974.

Yeh TC. 1950. The circulation of the high tropopause over China in the winter of 1945–1946. *Tellus* **2**: 173–183.